DOI: 10.1002/asia.200600410

Conformational Polymorphism in *N*-(4′-methoxyphenyl)-3-bromothiobenzamide

Anastasiya Bashkirava,[a] Philip C. Andrews,*[a] Peter C. Junk,[a] Evan G. Robertson,[a] Leone Spiccia,[a] and Nafty Vanderhoek[b]

Abstract: Three conformational polymorphs of *N*-(4′-methoxyphenyl)-3-bromothiobenzamide, yellow α, orange β, and yellow γ, have been identified by single-crystal X-ray diffraction. The properties and structure of the polymorphs were examined with FT Raman, FTIR (ATR), and UV/Vis spectroscopy, as well as differential scanning calorimetry. Computational data on rotational barriers in the isolated gas-phase molecule indicate that the molecular conformation found in the α form is energetically preferred, but only by around 2 kJ mol^{-1} over the γ conformation. The planar molecular structure found in the β form is destabilized by 10–14 kJ mol^{-1}, depending on the calculation method. However, experimental evidence suggests that the β polymorph is the most stable crystalline phase at room temperature. This is attributed to the relative planarity of this structure, which allows more and stronger intermolecular interactions, that is, more energetically effective packing. Calculated electronic-absorption maxima were in agreement with experimental spectra.

Keywords: conformation analysis · phase transitions · polymorphism · thiobenzamide · X-ray diffraction

Introduction

Although polymorphism in crystalline materials is a relatively common phenomenon,[1] its importance in modern-day chemistry cannot be overstated. Medicinal chemists, theoreticians, crystal engineers, and materials scientists all expend significant amounts of time and resources in attempting to understand and control the polymorphic properties of substances.[2]

The arrangement of relatively rigid molecules in different crystal forms through different intermolecular interactions is called packing polymorphism (e.g., as observed for *o*-anisaldehyde[3] and 3-acetylcoumarin).[4] In contrast, conformational polymorphism arises when less-rigid molecules fold into different crystal forms.[5,6] The delicate balance of forces required for this phenomenon is illustrated by the fact that the conformation itself determines the availability of functional groups for intermolecular interactions, that is, through crystal packing, but the molecular surroundings, as regulated by packing, ultimately impact back on the adopted conformation. It is this combination of both conformational and packing features in producing particular energy minima that gives rise to observed polymorphic modifications.

Conformational polymorphism can arise when intermolecular interaction energies are comparable to those required for intramolecular rotation around single bonds.[2] However, Allen et al. claimed that conformations associated with strain energies of more than 4.2 kJ mol^{-1} are rarely observed in crystal structures.[7] Exceptions to this can occur when the high-energy gas-phase conformation is stabilized in the crystal by enhanced intermolecular interactions: the "systematic effect". The classic example of this is *ortho*-substituted biphenyls that have a close-to-planar conformation in the crystal phase as opposed to a 40° twist in the gas phase.[8] The subtle changes in both molecular geometry and intra- and intermolecular bonding when conformational polymorphism occurs have also been invoked to explain the different colors that often accompany different single crystals of a particular compound.[9,10]

In this paper, we report the discovery and study of three crystalline polymorphs of *N*-(4′-methoxyphenyl)-3-bromothiobenzamide (TBA), a compound with known biological

[a] A. Bashkirava, Dr. P. C. Andrews, Prof. P. C. Junk, Dr. E. G. Robertson, Prof. L. Spiccia
School of Chemistry, CRC Smartprint
Monash University
Clayton, Victoria 3800 (Australia)
Fax: (+61) 3-99054597
E-mail: phil.andrews@sci.monash.edu.au

[b] Dr. N. Vanderhoek
Ensis-Papro, CSIRO,
Bayview Avenue, Clayton, Victoria 3169 (Australia)

activity (antimicrobacterial, antituberculotic).[11–13] Although polymorphism has previously been reported for related *N*-phenylthiobenzamides,[14,15] at that time only IR analysis was conducted and discussed. Given the current interest in, and significance of, polymorphism in modern drug design and delivery,[16–19] particularly in the area of solubility, we undertook a more wide-ranging study that examined TBA conformational polymorphism by employing X-ray crystallography as well as FT Raman and FTIR (attenuated total reflection; ATR) spectroscopic techniques. In doing so, we endeavored to uncover the thermodynamic relationship between the three polymorphs. Furthermore, we also sought to gain an understanding of the effects of conformation on electronic absorbance spectra, stability, and the interconversion of polymorphic modifications by using UV/Vis spectrometry and quantum-chemical calculations.

Results and Discussion

Crystal Structures

Three crystal polymorphs were found for TBA. The α form was produced by crystallization of the freshly synthesized amorphous material from concentrated solutions in polar or nonpolar solvents (mesitylene, hexane, alcohols, acetone) as yellow prisms or needles, whereas the β form was obtained as orange plates on slow crystallization from more-dilute solutions in alcohol (EtOH, MeOH, EtOH/acetone, MeOH/acetone). When the solutions were left at room temperature, the initially formed yellow crystals became orange within one week. Upon isolation and drying in air, the orange crystals appeared to be stable indefinitely.

The γ form was obtained as yellow hexagonal plates in a mixture with the α and β forms by fast crystallization from acetone. Crucially here, all the solvent needed be removed, otherwise the γ form converted into the β. All forms of TBA displayed thermochromism and turned red on melting. The crystal structures of the three polymorphs were determined by single-crystal X-ray diffraction and are shown in Figures 1–3. The structures are shown projected in the plane of the methoxy-substituted aromatic ring, with the methyl group projecting out of the page. A summary of the details of the data collection and refinement are listed in Table 1.

A comparison of relevant bond angles and bond lengths is provided in Table 2. As expected, there is very little difference in bond length between all four (α_1, α_2, β, γ) of the molecular arrangements. However, it is in the angular arrangement and the degree of delocalization of the thioamide moiety relative to the two phenyl rings and the Br atom that we expect to observe significant differences.

It is noteworthy that the α_1 and α_2 molecules are slightly different. For the former, the C1–N1–C8 angle is slightly more obtuse (127.7(2)°) than in the latter (126.1(2)°), indicating a marginal decrease in the sp^2 character of the N atom. This is accompanied by a widening of the C9–C8–N1 angle in α_1 (122.5(2)°) relative to that in α_2 (120.9(2)°). In both α and β forms the central thioamide fragment (C2–C1–N1–C8) is essentially planar (dihedral angles: α_1 178.7(2), α_2 178.2(2), β 179.1(10)°), whereas the γ form displays a significant deviation from planarity (γ 174.5(2)°). Furthermore, all four molecular arrangements adopt the most energetically favorable *trans* conformation around the thioamide group.[20]

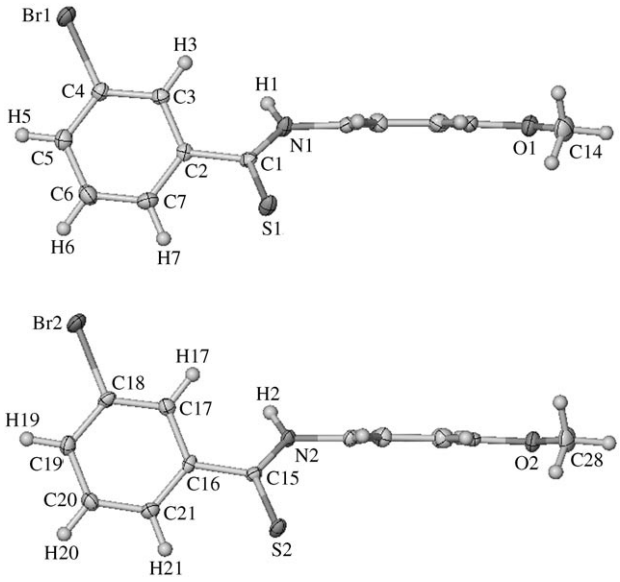

Figure 1. The two molecules α_1 (top) and α_2 (bottom) found in the asymmetric unit of the α form of TBA. Thermal ellipsoids are shown at 50% probability. A comparison of selected bond lengths and angles are given in Table 2.

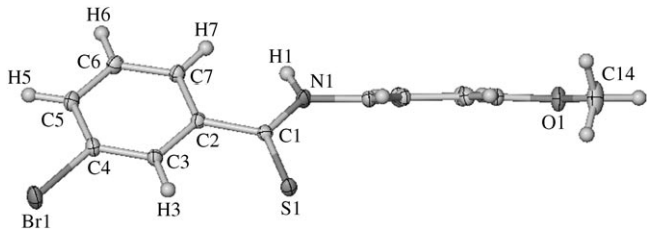

Figure 2. The β form of TBA. Thermal ellipsoids are shown at 50% probability. A comparison of selected bond lengths and angles are given in Table 2.

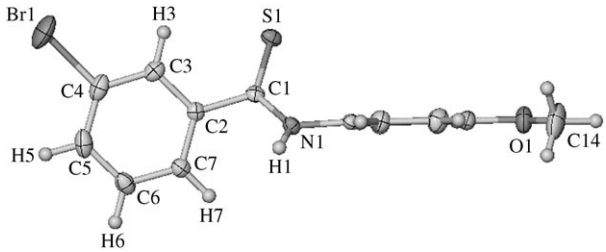

Figure 3. The γ form of TBA. Thermal ellipsoids are shown at 50% probability. A comparison of selected bond lengths and angles are given in Table 2.

Table 1. Crystal data for the three polymorphic forms of TBA.

	α[a]	β	γ
Crystal habit	yellow needle	orange plate	yellow plate
Empirical formula	$C_{14}H_{12}BrNOS$	$C_{14}H_{12}BrNOS$	$C_{14}H_{12}BrNOS$
M_r	322.22	322.22	322.22
Crystal system	orthorhombic	monoclinic	orthorhombic
Space group	$Pca2_1$	$P2_1/c$	$Pccn$
a [Å]	9.3827(3)	5.8266(5)	12.8747(6)
b [Å]	14.5368(5)	7.4723(6)	28.1304(11)
c [Å]	19.4967(7)	29.433(2)	7.4809(3)
β [°]	90	90.539(4)	90
V [Å^3]	2659.24(16)	1281.38(18)	2709.4(2)
Z	8	4	8
ρ_{calcd} [g cm^{-3}]	1.610	1.670	1.580
μ [mm^{-1}]	3.235	3.357	3.175
$F(000)$	1296	648	1296
Crystal size [mm]	0.14×0.08×0.03	0.12×0.10×0.05	0.10×0.10×0.03
θ range [°]	2.58–35.10	1.38–42.72	2.69–30.11
Reflections collected	29193	69157	48951
Independent reflections	10643 [R(int) = 0.0498]	9264 [R(int) = 0.1421]	3985 [R(int) = 0.0344]
Data/restraints/parameters	10643/1/335	9264/0/168	3985/0/168
Goodness-of-fit on F^2	0.943	0.981	1.042
Final R indices [$I > 2\sigma(I)$]	R_1 = 0.0438, wR_2 = 0.0793	R_1 = 0.0379, wR_2 = 0.0921	R_1 = 0.0369, wR_2 = 0.0757

[a] Absolute Flack parameter = 0.000(6).

Table 2. Selected bond lengths (Å) and angles (°) for the four solid-state molecular structures found for TBA.

	α_1	α_2[a]	β	γ
Br1–C4	1.901(3)	1.898(2)	1.899(1)	1.895(2)
S1–C1	1.673(3)	1.671(2)	1.675(1)	1.674(2)
O1–C11	1.365(3)	1.367(3)	1.362(1)	1.365(2)
O1–C14	1.429(3)	1.429(3)	1.424(1)	1.420(3)
N1–C1	1.339(3)	1.335(3)	1.337(1)	1.332(3)
N1–C8	1.422(3)	1.426(3)	1.423(1)	1.431(3)
C1–C2	1.486(4)	1.491(4)	1.497(1)	1.488(3)
C11–O1–C14	117.7(2)	117.0(2)	117.29(9)	117.4(2)
C1–N1–C8	127.7(2)	126.1(2)	128.29(9)	127.4(2)
N1–C1–C2	115.0(2)	115.8(2)	115.23(8)	114.9(2)
N1–C1–S1	126.4(2)	125.3(2)	123.02(8)	125.1(2)
C2–C1–S1	118.6(2)	118.9(2)	121.73(7)	120.0(2)
C7–C2–C1	119.4(2)	120.4(2)	122.90(9)	121.0(2)
C3–C2–C1	120.5(2)	120.5(2)	118.56(8)	119.5(2)
C13–C8–N1	118.2(2)	119.7(2)	122.59(9)	120.9(2)
C9–C8–N1	122.5(2)	120.9(2)	117.48(9)	119.0 (2)
O1–C11–C12	115.4(2)	116.0(2)	124.81(9)	115.3(2)
O1–C11–C10	125.2(2)	124.3(2)	115.28(9)	124.9(2)

[a] For α_2, the corresponding bond lengths and angles are listed, for example, the Br2–C18 bond corresponds to Br1–C4.

If we consider that the molecules can be described by three ring planes, one defined by the bromo-substituted phenyl ring (plane 1), the second by the thioamide group (N–C–S) (plane 2), and the third by the methoxy-substituted phenyl ring (plane 3), then each polymorph can be described by the internal relationship of these planes. A summary of the key dihedral angles is given in Table 3. Planes 1 and 3 are considerably rotated from plane 2 in the α and γ forms to give significant twist within each molecule, which contrasts with the β polymorph, in which planes 1 and 2 are almost coplanar, thereby making most of the molecule almost flat. The close proximity of H1 and H7 in this planar β arrangement is an energetically unfavorable arrangement. It results in a C7–C2–C1 angle that is relatively more obtuse and a C3–C2–C1 angle that is more acute that in the other forms (Table 2). The overall stability of this β form must therefore derive from other intermolecular-bonding considerations.

Table 3. Dihedral angles (°) for the three planes (PhBr = plane 1, N–C–S = plane 2, MeOPh = plane 3) in each molecule found in the three polymorphs of TBA.

	α_1	α_2	β	γ
Planes 1 and 2	43.3(3)	35.1(3)	4.73(9)	40.0(2)
Planes 2 and 3	37.5(4)	42.8(3)	58.0(2)	64.4(3)
Planes 1 and 3	76.5(2)	77.8(2)	55.7(1)	69.8(3)

The out-of-plane deviation of the S atom observed in the γ form, which relates to the observed difference in the dihedral angle for planes 1 and 2 in the β and γ forms, is shown in Figure 4. The higher-energy arrangement in β, with sterically crowded coplanar Br, H, and S atoms, is most likely compensated for by the stabilization energy gained from more-efficient electron delocalization.

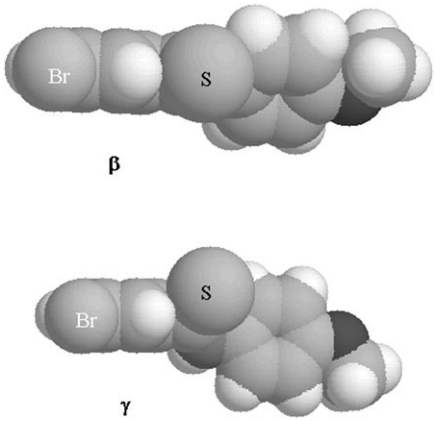

Figure 4. Space-filling representation of the β and γ forms showing the significant out-of-plane deviation of the S atom in the γ form.

Crystal packing in the polymorphs is largely, though not exclusively, determined by intermolecular hydrogen bonding between N–H and C–H with S and O atoms, respectively. The relevant bonding distances are given in Table 4. However, the different conformations of the polymorphs understandably result in, and in part derive from, a variance in the availability of the various functional groups to engage in hydrogen bonding, and, for the delocalized systems, other weaker noncovalent interactions such as van der Waals attraction. Both α_1 and α_2 molecules build up two separated chains of molecules by means of N–H···S hydrogen bonds of 2.50(3) Å for α_1 and 2.59(3) Å for α_2. The chains of one type

CHEMISTRY
AN ASIAN JOURNAL

Table 4. Intermolecular bonding distances (Å) and angles (°) in the polymorphic forms of TBA.

	α_1	α_2	β		γ
N–H···S	2.50(3)	2.59(3)	2.80(2)	2.96(2)[a]	2.57(3)
N···S	3.368(2)	3.330(2)	3.415 (1)	3.646(1)[a]	3.355(2)
∢NH···S	157(3)	155(3)	127.0(2)	135.(2)[a]	158(2)
C14···O[b]			3.334(2)		3.340(3)
∢C14HO			143.0		129.6
π–π (plane 1 to 3)			3.272–3.418		
centroid···centroid			3.713		
∢plane 1 to 3			3.12(0.05)		
π–π (plane 1 to 1)					3.483–3.510
centroid···centroid					3.744
∢plane 1 to 1					0.57(0.08)

[a] Hydrogen bonds between 2D layers. [b] H atoms on methyl groups placed in optimized positions (C–H, average 0.95 Å).

are linked by C–H···O bonds to the nonequivalent layer (either α_1 or α_2). Only weak van der Waals forces hold alternate layers together (Figure 5). An analysis of the intermolecular bonding distances suggests that the α_2 layers form weaker interactions than α_1.

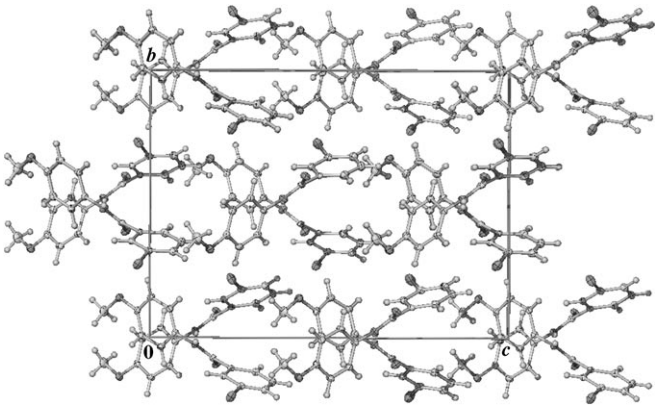

Figure 5. Crystal packing and unit-cell diagram of the α polymorph, showing the α_1 layer sandwiched between the α_2 layers.

In comparison to the α conformation, the molecular structure of the β form is relatively planar, which allows more dense packing as reflected in the cell volume and crystal density (Table 1). In the simple 1D chain structure, the molecules orientate themselves in a "head-to-head" and "tail-to-tail" arrangement through relatively strong hydrogen bonding between the OCH_3 groups and weaker, but still significant, C–H···Br bonding.[21] The chains are then assembled into a layer structure through weak N–H···S bonding and offset face-to-face π–π stacking (Figure 6). Finally, a second N–H···S bond and weak Br···Br interactions (calculated distance 3.676 Å, sum of van der Waals radii (Br–Br) 3.7 Å)[22–24] between layers form a well-defined 3D framework.

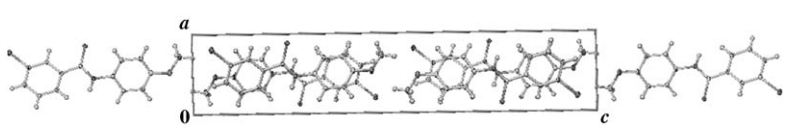

Figure 6. Crystal packing and unit-cell diagram of the β polymorph, shown along the short *b* axis.

In the γ form, columns are created by codirectional N–H···S and π···π interactions (C8–C13 rings), which then pack together through alternating "head-to-head" hydrogen-bonding OCH_3 groups and "tail-to-tail" CH···Br interactions. The 3D structure (Figure 7) is then constructed by these column layers stacking through directional C–H···Ph bonding (average 2.755 Å).

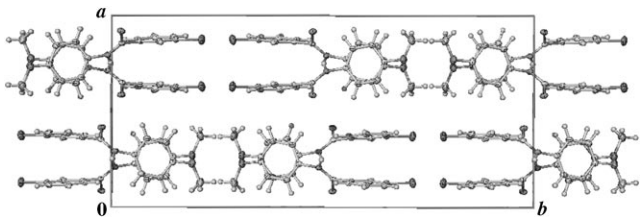

Figure 7. Crystal packing and unit-cell diagram of the γ polymorph, shown along the short *c* axis.

Vibrational Spectra

The FTIR (ATR) and Raman spectra of the three polymorphs are compared in Figures 8 and 9, respectively. Though not shown here, the spectra obtained on heating the β form to 90 °C for 5 min were identical to those obtained for the γ form. The peak positions and intensities clearly show differences among the species, thus confirming that the three forms are distinct structures. In the ATR spectra, the main differences were observed in the N–H stretching region, which supports the variation in intermolecular hydrogen bonding seen in the crystal structures. The data in Table 4 suggests that the N–H···S hydrogen bonding is weaker in the β form; the NH···S and N···S distances are longer than those found in the α and γ forms, and the N–H···S angles deviate further from linearity. This is in accordance with the observation that the N–H stretching vibration in the β polymorph appeared at a higher wavenumber value (3284 cm^{-1}) than for the other two polymorphs (3174 and 3157 cm^{-1}). The Raman spectra of the three polymorphs differ even more than their IR spectra. Conformational differences may be reflected in both

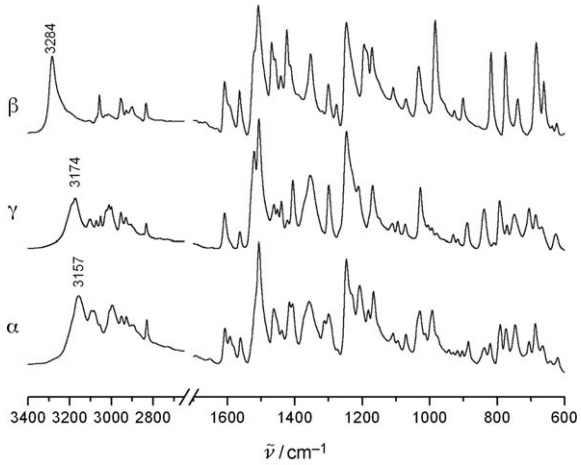

Figure 8. FTIR (ATR) spectra of the α, β, and γ polymorphs of TBA.

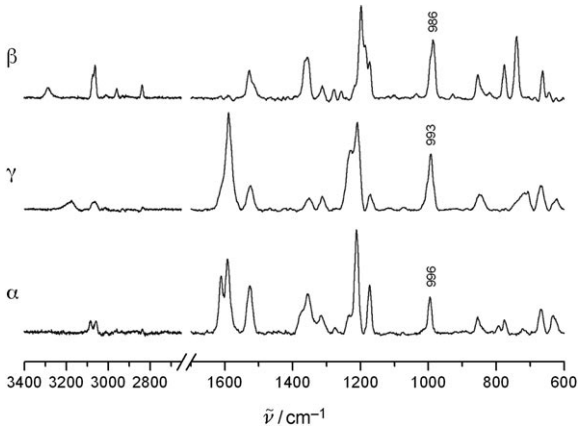

Figure 9. Raman spectra of the α, β, and γ polymorphs of TBA.

types of spectra, but the polarizability of bonds that gives rise to Raman intensity is more sensitive to subtle effects of molecular alignment and orientation and of long-range intermolecular interactions.

Interconversion of the Forms: DSC Study

To establish some understanding of the relationship between the polymorphs and their stability, differential scanning calorimetry (DSC) studies were conducted on the various crystal forms. The DSC patterns of the pure single crystals of the three polymorphs are shown in Figure 10 and Table 5.

The DSC traces of the α and γ polymorphs show only the sharp endothermic peaks associated with melting (Figure 10). In contrast, the β polymorph undergoes an endothermic transition to the γ form before the onset of melting. The thermodynamic data derived from the DSC traces for the three crystal forms are summarized in Table 6.

On the basis of the rules for enantiotropy and monotropy developed by Bürger and Ramberger,[25] we can conclude that the β and γ polymorphs are enantiotropic (Figure 11 b).

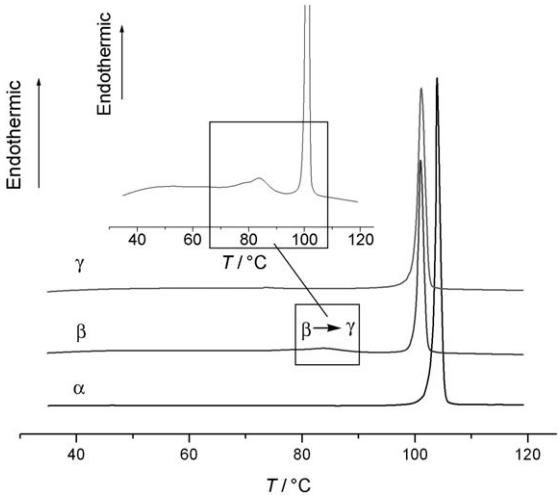

Figure 10. DSC data of the single crystals of the three polymorphs.

Table 5. DSC data summary for the crystalline polymorphs of TBA.

	α	β	γ
M.p. [°C]	103.5 ± 0.4[a]	–	100.0 ± 0.2[b]
Enthalpy of fusion [kJ mol^{-1}]	28.5 ± 0.7[a]	24.7[c]	22.6 ± 0.2[b]
β→γ Transition temperature [°C]		74 ± 2	74 ± 2
β→γ Transition enthalpy [kJ mol^{-1}]		2.1 ± 0.1[d]	

[a] $n=6$. [b] $n=4$. [c] Calculated from the heat-of-fusion rule $\Delta H_f^{\beta} \approx \Delta H_f^{\gamma} + \Delta H_t^{\beta-\gamma}$. [d] $n=6$. n is the polynomial used in the calculation.

Table 6. Structural, energetic, and spectral properties for single molecules of the α, β, and γ conformers calculated by ab initio methods.

	Method	α_1	α_2	β	γ
E_{rel} [kJmol^{-1}]	MP2[a]	0.0	0.0	14.4	1.9
	B3LYP[b]	0.0	0.0	10.1	2.4
S1–C1–C2–C3	observed[c]	135.8(2)	145.4(2)	−3.0(1)	−39.6(2)
	MP2[a]	137.8	137.8	−3.0[d]	−41.9
	B3LYP[b]	136.9	136.9	−3.0 d	−39.9
C1–N1–C8–C_{ortho}[e]	observed[c]	−44.3	−50.3	−48.1	131.4
	MP2[a]	−39.4	−39.4	−49.8	137.9
	B3LYP[b]	−12.7	−12.7	−37.7	149.8
$S_1 \leftarrow S_0$ origin [nm]	TDDFT[f]	441.6	441.6	478.0	442.1
	TDDFT[g]	440.4	440.4	479.1	447.6
$S_2 \leftarrow S_0$ origin [nm]	TDDFT[f]	344.8	344.8	372.9	342.3
	TDDFT[g]	343.7	343.7	370.4	344.8

[a] MP2/6-31G(d,p)-optimized geometry. [b] B3LYP/6-311+G(d,p)-optimized geometry. [c] Experimental value. [d] τ_{SCCC} constrained to 3° for all ab initio structures of β. [e] C_{ortho} is the C atom of the C8–C13 ring *ortho* to the thioamide group and closest to the methyl group. [f] TDDFT B3LYP/6-31G(d,p) carried out at MP2/6-31G(d,p)-optimized geometry. [g] TDDFT B3LYP/6-31G(d,p) carried out at B3LYP/6-311+G(d,p)-optimized geometry.

Below the thermodynamic transition point (β→γ), the β polymorph is thermodynamically more stable and less soluble, whereas the same applies to the γ polymorph above this point (Figure 11 b). The evidence is as follows:

1) Enthalpy-of-transition rule: The endothermic transition of β to γ was observed at (74.2 ± 2.0) °C (so the actual

CHEMISTRY
AN ASIAN JOURNAL

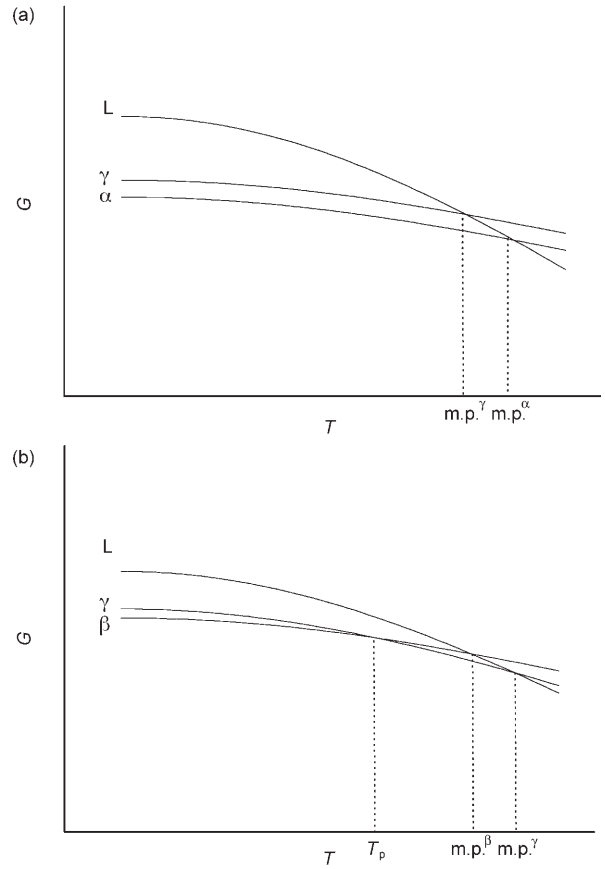

Figure 11. Schematic diagram of the dependence of Gibbs free energy on temperature. a) Monotropy of α and γ polymorphs. b) Enantiotropy of β and γ polymorphs.

thermodynamic transition point lies below that temperature), that is, the forms are related enantiotropically. Moreover, it may be inferred that the melting point of β should be lower than that of γ.

2) Enthalpy-of-fusion rule: Although no melting of the β form could be detected and so measurement of the corresponding enthalpy of fusion was not possible, the approximate enthalpy of fusion was calculated as $\Delta H_f^{\beta} \approx \Delta H_f^{\gamma} + \Delta H_t^{\beta-\gamma}$.

3) Density rule: Generally, the densest crystal should be the most stable at absolute zero temperature. If the polymorph with the higher melting point has a density less than the polymorph with the lower melting point, then they are enantiotropic.[25] From the X-ray data (Table 1), the density of the β form is higher than that of the γ form, thus indicating enantiotropy.

4) Solution-mediated transition: The conversion of the yellow γ crystals into the orange β crystals in the presence of solvent at ambient temperature indicates that the γ form is metastable at this temperature, whereas the β form is stable.

Notably, we cannot reliably apply the rule based on IR studies (rule 5), as it was reported by Bürger and Rambergerer[25] that there is significant deviation and uncertainty in its application to carbamides;[26] thus, we made the assumption that this most likely also applies to thioamides.

In contrast, the α and γ polymorphs are considered to be monotropically related. The α polymorph is more stable and less soluble than the γ form regardless of temperature (Figure 11 a). This conclusion is supported by the following arguments:

1) Enthalpy-of-fusion rule: As the higher-melting-point polymorph (α) has a higher enthalpy of fusion (Table 5) than the lower-melting-point γ polymorph, the relationship between them is monotropic.

2) Density rule: The α polymorph with the higher melting point also has a higher density than the γ polymorph, so they represent a case of monotropy.

Finally, we considered the possible transition between α and β. At room temperature, yellow α (and γ) crystals slowly converted into the orange β crystals in the presence of solvent, thus indicating that the β form is the most stable. According to the energy diagram (Figure 11 a), after the β→γ conversion point the most stable conformation is α. Theoretically, the relationship between α and β forms should be enantiotropic, with the α form more stable at higher temperatures; it is clear from the DSC data that the α form is indeed the most stable from 74 °C until it melts, which raises the question of why no interconversion was observed between the α and β forms in the DSC experiments. The answer may lie in the torsion of the brominated ring with respect to the thioamide required to convert between these forms. The transition from β to α requires a rotation in the dihedral angle S1−C1−C2−C3 from about 3° (−3°) to about 135°(−135°). The molecule cannot do this without rotating through 40° (−40°), which corresponds to the γ form (Figure 12). Therefore, direct solid-phase transition of the α phase to the β phase, and vice versa, must be mediated by the γ phase.

Computational Study

Ab initio calculations were performed by using the Gaussian 03 suite of programs.[27] Geometry optimizations were performed with the Moller–Plesset second-order perturbation, MP2/631G(d,p), and density functional theory at the B3LYP/6311+G(d,p) level. In each case, structures were computed for single molecules, so that the data obtained relates to the intrinsic conformational preferences in the absence of intermolecular interactions. Computed properties are summarized in Table 6. A key geometric parameter that distinguishes the conformers is the dihedral (torsion) angle S1−C1−C2−C3, related to the angle between planes 1 and 2 in Table 3, which defines the planarity of the thioamide group with respect to the Br-substituted phenyl group. Relaxed-potential-energy scans reveal two distinct potential-energy minima (and two that are equivalent by symmetry) with S1−C1−C2−C3 twisted some 40° from planarity (Figure 12). These minima correspond very closely to the values of S1−C1−C2−C3 found in crystal structures of conformers α and γ, with the α form preferred by around

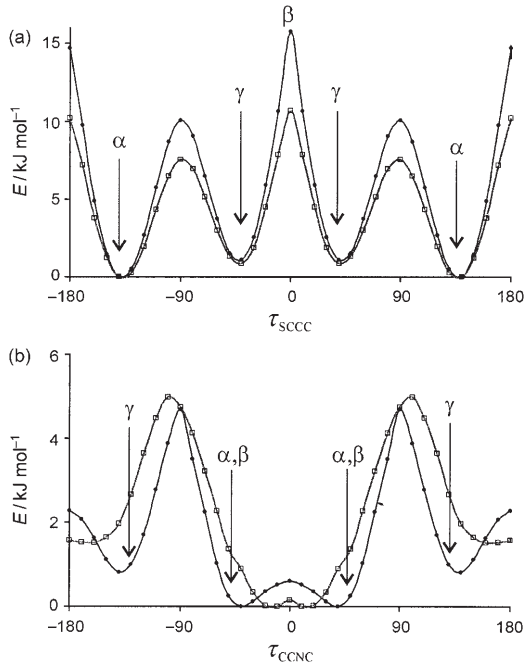

Figure 12. Relaxed potential energy versus a) τ_{SCCC} (S1−C1−C2−C3) and b) τ_{CCNC} (C_{ortho}−C8−N1−C1; C_{ortho} is the C atom *ortho* to the thioamide group and closest to the methyl group) at the MP2/6-31G(d,p) (●) and B3LYP/6-311+G(d,p) (□) levels. The values of τ_{SCCC} corresponding to the α, β, and γ isomers are marked.

2 kJ mol^{-1} at both levels of theory. The barrier to planarity of S1−C1−C2−C3 is considerable, around 16 kJ mol^{-1} at the MP2/6-31G(d,p) level or 10 kJ mol^{-1} at the B3LYP/6311+G-(d,p) level. This is a significant result given that the crystal structure of the β conformer has a near-planar arrangement with the S1−C1−C2−C3 angle at −3°. To compute properties of the β conformer, it was necessary to constrain S1−C1−C2−C3 to −3°.

The dihedral angle that defines planarity of the thioamide group with respect to the methoxy-substituted C8−C13 ring is C1−N1−C8−C9 or C1−N1−C8−C13. The relevant relaxed-potential-energy scans are shown in Figure 12b. The values of τ_{CCNC} corresponding to potential minima at the MP2 level are around 40–50° degrees from planarity, which is very close to those of the crystal structures. The agreement with the B3LYP values is not so favorable, but both levels of theory indicate that the barriers to planarity are insignificant, in marked contrast to the situation with the Br-substituted ring.

The crystal structures of the α and γ forms are very close to the computed potential-energy minima of the isolated (gas-phase) molecules, whereas the β (orange) structure has around 15 kJ mol^{-1} (MP2 level) of "strain" associated with the planar S1−C1−C2−C3 arrangement. For the β form to be thermodynamically competitive, it must have more-favorable intermolecular interactions owing to crystal-packing considerations. In particular, it is evident that π–π stacking is optimal in the β form (the distance between rings is around 3.42 Å; compare the separation between layers of graphite of 3.35 Å). Stronger intermolecular forces imply that low-frequency vibrations (both lattice and molecular modes) are more hindered, and therefore the vibrational entropy is smaller for the β form. This explains the observed enantiotropic behavior and the preference for the yellow α and γ forms at higher temperatures.

Electronic spectral properties were computed by using time-dependent density functional theory (TD-DFT) at the B3LYP/6-31G(d,p) level. These are single-point calculations performed at the ground-state geometries, as specified in Table 6. The $S_1 \leftarrow S_0$ and $S_2 \leftarrow S_0$ origin transitions of the α and γ conformers are virtually identical. The key finding, however, is that these transitions are shifted to lower energy (higher wavelength) in the β structure relative to the α and γ conformers by around 37 and 28 nm, respectively. These $\pi^* \leftarrow \pi$ transitions are associated with the Br-substituted ring. The underlying reason for the spectral shifts is the increased planarity of the thioamide group with respect to the Br-substituted ring, and the enhanced π conjugation that results. In contrast, the planarity of the thioamide group with respect to the methoxy-substituted ring has very little influence on the spectrum, as may be seen by comparison of the TD-DFT results for MP2- and B3LYP-optimized α and γ structures in Table 6.

UV/Vis Spectra

The diffuse reflectance spectra of the α and β polymorphs of TBA ground with dried KBr are shown in Figure 13. The long-wavelength transition is shifted to lower energy by about 50 nm in the orange β form with respect to the yellow α form. The band origins predicted from TD-DFT calculations are also shown in Figure 13. Their positions and the red shift observed for the β polymorph are consistent with the observed spectra. The color difference between the β

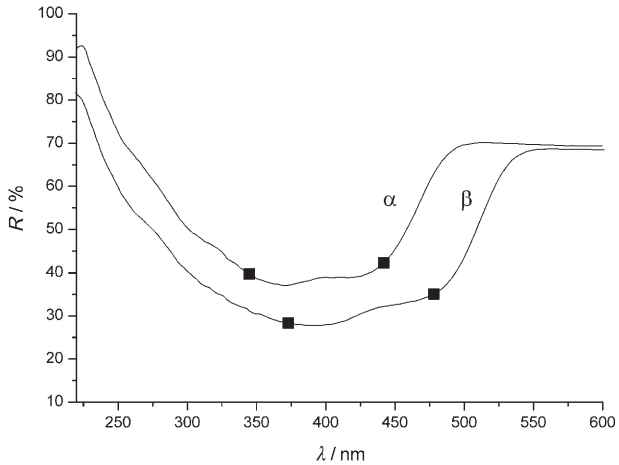

Figure 13. Diffuse reflectance spectra of the α and β polymorphs. The square symbols represent the theoretically calculated transition wavelengths (TDDFT B3LYP/6-31G(d,p) carried out at MP2/6-31G(d,p)-optimized geometry) for each polymorph.

polymorph and the α and γ forms may therefore be attributed to conformationally based spectral shifts.

Conclusions

We have discovered three polymorphic forms of *N*-(4′-methoxyphenyl)-3-bromothiobenzamide and conclude from both experimental and computational studies of the three polymorphs (α, β, and γ) that they represent conformational polymorphism. The main difference between the conformations is in the dihedral angles S1−C1−C2−C3. In the β form, the C=S bond is almost coplanar with the Br-substituted phenyl ring. All three polymorphs display different crystal packing arising from various hydrogen-bonding modes (N−H···S, C−H···O) and other nonclassical weak covalent interactions (π–π stacking and C−H···π). The β form, which displays the greatest degree of planarity, is the most dense and efficiently packed form. The conformational and packing differences revealed by the crystal data were confirmed by FTIR (ATR) and FT Raman experiments, showing the distinct variations in the N−H stretching region and the vibrations of the thioamide group. The thermodynamic rules established for polymorphic crystals and the DSC data showed that the α (m.p. (103.5 ± 0.4) °C) and γ (m.p. (100.0 ± 0.2) °C) forms are monotropically related, with the α form being more stable and less soluble. In contrast, the β and γ forms are enantiotropic. The γ form is more stable than the β form above the thermodynamic transition point and vice versa. Due to geometrical constraints, the transition between the β and α forms has to be mediated by the γ phase. Ab initio calculations correlated well with the observed experimental results. The S1−C1−C2−C3 dihedral angle of the α conformer is in good agreement with the potential-energy minimum calculated for the isolated, gas-phase molecule, whereas the corresponding dihedral angle for the γ conformation represents another energy minimum that is less favorable by about 2 kJ mol^{-1}. The dihedral angle found in the β form (3°) is very close to the potential-energy maximum at 0°, that is, 10–15 kJ mol^{-1} higher in energy. However, the experimental evidence demonstrates that the orange β form is the most stable crystalline phase at room temperature. Therefore, TBA is one of the rare examples of the systematic effects of crystal-packing forces favoring a different form from the stable gas-phase conformation. The observed color differences between the yellow α and γ forms and the orange β form can be explained by the coplanarity of the C=S group and the Br-substituted phenyl ring, which results in enhanced conjugation of molecular orbitals and a consequent red shift of the π*←π absorption bands. According to the variations in structure and physical properties, the thermochromic color change upon melting can plausibly be explained by an increase in π–π interactions,[7,28] excitonic coupling via head-to-tail orientation of transition-dipole moments, or the stabilization of the more-polar β conformation in the melt.

Experimental Section

Single-crystal X-ray diffraction studies of the α, β, and γ forms of TBA were performed on a Bruker Apex II CCD diffractometer by using monochromated $Mo_{K\alpha}$ radiation ($\lambda = 0.71073$ Å). Data collection was undertaken at 123 K. The structures were solved by using direct methods with SHELXS-97[29] and refined by use of the X-seed interface for SHELX-97.[30] All non-hydrogen atoms were located and refined anisotropically. The H atoms on N were located and refined isotropically. All other hydrogen atoms were included at geometrically estimated positions and included in the final least-squares refinement. CCDC-630391–630393 contain the supplementary crystallographic data (excluding structure factors) for this paper. These data can be obtained free of charge from the Cambridge Crystallographic Data Centre, 12 Union Road, Cambridge CB2 1EZ, UK (fax: (+44) 1223-336-033; email: deposit@ccdc.cam.ac.uk) or at www.ccdc.cam.ac.uk/data_request.cif.

UV/Vis spectra of solutions in methanol were recorded on a Varian model Cary 100 Bio UV/Vis spectrophotometer. ATR-IR spectra were recorded in the range 3500–600 cm^{-1} on a Bruker IFS 55 FTIR spectrometer by using a Specac single reflection ATR system fitted with a single-bounce diamond top plate. On the latter instrument samples were recorded as solids pressed against a diamond crystal. Raman spectra were obtained on a Renishaw RM2000 spectrometer equipped with a 35-mW HeNe laser-excitation source and a Linkam FTIR hot/cold stage. DSC measurements were conducted with an STA 1500 instrument (Rheometric Scientific) under nitrogen atmosphere (50 mL min^{-1}) between 25 and 120 °C with a temperature-ramp rate of 2.5° min^{-1}. The instrument was calibrated by using four melting points (indium, tin, lead, zinc), and aluminium pans were used in all experiments. NMR spectra were recorded with a 300 MHz Bruker DPX-300 spectrometer, as solutions in the deuterated solvents specified. Chemical shifts (δ) were calibrated against the residual solvent peak. Mass spectra were recorded on a Brüker BioApex FT-ICRMS (Fourier Transfer Ion Resonance Mass Spectrometer) with an Analytica ESI source. Elemental analysis was performed by The Campbell Microanalytical Laboratory (Dunedin, New Zealand).

Synthesis: The bulk synthesis of TBA as an amorphous powder was carried out according to the described literature procedure.[31] Yield 73 %; ^{1}H NMR (300 MHz, [D$_6$]dimethyl sulfoxide ([D$_6$]DMSO), 30 °C): δ = 11.73 (br s, 1H, H1), 7.96 (s, 1H, H3), 7.81 (d, J = 7.8 Hz, 1H, H5), 7.74–7.70 (m, 3H, H7, H10, H12), 7.42 (t, J = 7.9 Hz, 1H, H6), 6.99 (d, J = 8.9 Hz, 2H, H9, H13), 3.79 ppm (s, 3H, H14A–H14C); ^{13}C NMR (75 MHz, [D$_6$]DMSO): δ = 55.3 (C14), 113.6 (C10, C12), 121.1 (C4), 125.5 (C9, C13), 126.5(C(7)), 129.8 (C8), 130.1 (C6), 132.8 (C3), 133.0 (C5), 144.4 (C2), 157.3 (C11), 194.5 ppm (C1); MS (ESI, +ve, MeOH): m/z (%) = 344.0 $[C_{14}H_{12}BrNOS+Na]^+$ (100), 322.0 $[C_{14}H_{12}BrNOS+H]^+$ (50.66), 378.0 $[C_{14}H_{12}BrNOS+Na+MeOH]^+$ (26.97); elemental analysis: calcd (%) for $C_{14}H_{12}BrNOS$: C 52.2, H 3.8, N 4.4; found: C 52.2, H 3.8, N 4.3.

Acknowledgements

We thank the Cooperative Research Centre for Functional Communication Surfaces (CRC Smartprint) and Monash University for financial support. Quantum-chemistry calculations were carried out at the Australian Partnership for Advanced Computing (APAC) National Facility. The Australian Research Council (LIEF grants scheme) and the Victorian Institute of Chemical Sciences are acknowledged for funding of the CCD X-ray diffractometer.

[1] T. L. Threlfall, *Analyst* **1995**, *120*, 2435.
[2] J. Bernstein, *Polymorphism in Molecular Crystals, 1st ed.*, Oxford University Press Inc., New York, **2002**, p. 410.
[3] J. N. Moorthy, R. Natarajan, P. Mala, P. Venugopalan, *New J. Chem.* **2004**, *28*, 1416.
[4] P. Munshi, T. N. G. Row, *Cryst. Growth Des.* **2006**, ***6***, 708.

[5] J. R. Smith, W. Xu, D. Raftery, *J. Phys. Chem. B* **2006**, *110*, 7766.
[6] C. Guo, M. B. Hickey, E. R. Guggenheim, V. Enkelmann, B. M. Foxman, *Chem. Commun.* **2005**, 2220.
[7] F. H. Allen, S. E. Harris, R. Taylor, *J. Comput. Aided Mol. Des.* **1996**, *10*, 247.
[8] C. P. Brock, R. P. Minton, *J. Am. Chem. Soc.* **1989**, *111*, 4586.
[9] L. A. Leites, S. S. Bukalov, J. E. Mangette, T. A. Schmedake, R. West, *Spectrochim. Acta Part A* **2003**, ***59***, 1975.
[10] L. Yu, *J. Phys. Chem. A* **2002**, *106*, 544.
[11] K. Kral'ova, F. Sersen, L. Kubicova, K. Waisser, *J. Trace Microprobe Tech.* **2000**, *18*, 251.
[12] K. Waisser, L. Kubicova, Z. Odlerova, *Collect. Czech. Chem. Commun.* **1993**, *58*, 205.
[13] K. Waisser, N. Houngbedji, M. Machacek, M. Sekera, J. Urban, Z. Odlerova, *Collect. Czech. Chem. Commun.* **1990**, *55*, 307.
[14] O. Grupce, I. Petrov, *J. Mol. Struct.* **1984**, *115*, 119.
[15] W. Geiger, J. Kurz, *Naturwissenschaften* **1967**, *54*, 564.
[16] S. J. Wieczorek, G. J. Tsongalis, *Clin. Chim. Acta* **2001**, *308*, 1.
[17] E. T. Maggio, M. Shenderovich, R. Kagan, D. Goddette, K. Ramnarayan, *Drug Discovery Today* **2002**, *7*, 1214.
[18] D. A. Snider, W. Addicks, W. Owens, *Adv. Drug Delivery Rev.* **2004**, *56*, 391.
[19] C. H. Schwalbe, *Crystallogr. Rev.* **2005**, *11*, 49.
[20] C. Aleman, *J. Phys. Chem. A* **2001**, *105*, 6717.
[21] G. Echeverría, A. Fantoni, J. Marañón, G. Punte, *Struct. Chem.* **2005**, *16*, 571.
[22] M. Kubicki, *Acta Crystallogr. Sect. B: Struct. Sci.* **2004**, *B60*, 333.
[23] C. M. Reddy, M. T. Kirchner, R. C. Gundakaram, K. A. Padmanabhan, G. R. Desiraju, *Chem. Eur. J.* **2006**, *12*, 2222.
[24] J. B.-J. Teh, P. S. Patil, H.-K. Fun, I. A. Razak, S. M. Dharmaprakashb, *Acta Crystallogr. Sect. E: Struct. Rep. Online* **2006**, *E62*, o2399.
[25] A. Bürger, R. Ramberger, *Mikrochim. Acta* **1979**, *72*, 259.
[26] A. Bürger, R. Ramberger, *Mikrochim. Acta* **1979**, *72*, 273.
[27] M. J. Frisch, G. W. Trucks, H. B. Schlegel, G. E. Scuseria, M. A. Robb, J. R. Cheeseman, J. A. Montgomery, Jr., T. Vreven, K. N. Kudin, J. C. Burant, J. M. Millam, S. S. Iyengar, J. Tomasi, V. Barone, B. Mennucci, M. Cossi, G. Scalmani, N. Rega, G. A. Petersson, H. Nakatsuji, M. Hada, M. Ehara, K. Toyota, R. Fukuda, J. Hasegawa, M. Ishida, T. Nakajima, Y. Honda, O. Kitao, H. Nakai, M. Klene, X. Li, J. E. Knox, H. P. Hratchian, J. B. Cross, V. Bakken, C. Adamo, J. Jaramillo, R. Gomperts, R. E. Stratmann, O. Yazyev, A. J. Austin, R. Cammi, C. Pomelli, J. W. Ochterski, P. Y. Ayala, K. Morokuma, G. A. Voth, P. Salvador, J. J. Dannenberg, V. G. Zakrzewski, S. Dapprich, A. D. Daniels, M. C. Strain, O. Farkas, D. K. Malick, A. D. Rabuck, K. Raghavachari, J. B. Foresman, J. V. Ortiz, Q. Cui, A. G. Baboul, S. Clifford, J. Cioslowski, B. B. Stefanov, G. Liu, A. Liashenko, P. Piskorz, I. Komaromi, R. L. Martin, D. J. Fox, T. Keith, M. A. Al-Laham, C. Y. Peng, A. Nanayakkara, M. Challacombe, P. M. W. Gill, B. Johnson, W. Chen, M. W. Wong, C. Gonzalez, J. A. Pople, Gaussian 03, Revision C.02, Gaussian, Inc., Wallingford, CT (USA), **2004**.
[28] P. U. Biedermann, J. J. Stezowski, I. Agranat, *Chem. Eur. J.* **2006**, *12*, 3345.
[29] G. M. Sheldrick, SHELX-97, Program for the Solution of Crystal Structures, University of Göttingen, Göttingen (Germany), **1997**.
[30] L. J. Barbour, XSEED: A Graphical Interface for Use with the SHELX-97 Program Suite, University of Missouri, Columbia, MO (USA) **1999**.
[31] C. A. Mathis, Y. Wang, D. P. Holt, G-F. Huang, M. L. Debnath, W. E. Klunk, *J. Med. Chem.* **2003**, *46*, 2740.

Received: December 11, 2006

